Characterization of Induced Seismicity in a Petroleum Reservoir: A Case Study

Edmond Sze, M. Nafi Toksöz, and Daniel R. Burns
Earth Resources Laboratory
Dept. of Earth, Atmospheric and Planetary Sciences
Massachusetts Institute of Technology
Cambridge, MA 02139

Abstract

Fluid production and injection in hydrocarbon and geothermal reservoirs generally results in induced seismic activity. In this paper we study the microseismic activity in a petroleum field in Oman. The microearthquake data we used are those collected by a five-station digital network in the field between 29 October 1999 and 18 June 2001. We relocated 405 high-quality microseismic events using P and S travel-times picked from waveform data by the global grid-search location method. The results reveal a complex seismic zone with a NE-SW trend. All events are located within a depth range of 0.5 to 3.5 km. Focal mechanisms of 10 events of magnitude greater than one are inverted using the wavelet-based waveform inversion method where the source parameters, data kernel, waveform data, and the inversion are all represented by wavelet expansions. The dominant style of focal mechanism is left-lateral strike-slip for events with focal depths less than 1.5 km, and dip-slip along an obliquely trending fault for those with focal depths greater than 2.0 km. The inferred focal plane is nearly vertical and has a strike of NE-SW, which is also consistent with the trend of seismicity. To determine the cause of the events, seismicity rate is correlated with gas production and fluid injection. The results show that event rate in the field is strongly correlated with gas production in the Natih formation.

1.   Introduction

Microseismic monitoring has been conducted in an oil and gas field in north-central Oman by the Petroleum Development Oman (PDO) since 1996. The petroleum field is located in the Fahud Salt Basin (Figure 1a) and is one of the largest producing fields in the country. Producing reservoirs occur in two carbonate formations – the Natih and the Shuaiba. Induced microseismicity associated with the fault / fracture networks provide useful knowledge of their structural details, fluid flow paths, and dynamics properties that are valuable for reservoir development and geomechanical modeling.

In this study, data collected on the passive seismic network have been used to further understand the reservoir by: 1) locating hypocenters to identify active faults / fractures in the reservoir, 2) inferring reservoir fault mechanics by waveform inversion for moment tensor, and 3) correlating between seismic activity and fluid projection / injection operations.

2.   Data

Induced microearthquake waveform data were collected by five downhole arrays installed by the PDO (Figure 1b). Each array is 15 m long with four three-component, 4.5 Hz geophones cemented on the well-bore. The four geophones were placed at each borehole at 135 m, 140 m, 145 m, and 150 m depths. A three-component geophone has an orthogonal configuration with two horizontal components and one vertical component.

All data used for this study were collected from October 29, 1999 to June 18, 2001. Data sampling rate is 125 Hz. We select events recorded by at least four stations with distinctive P- and S-arrivals. A total of 405 high-quality events occurring in the reservoir out of 802 events detected by the network are selected for the period.

3. Location Estimates

Seismograms are first rotated into vertical, radial, and transverse components assuming straight raypaths from the stations to the preliminary estimates of source locations. Then, we repicked the corresponding P, S arrival time, and estimated the locations of 405 microearthquakes using NonLinLoc, a non-linear, global search method (Lomax et al., 2000). It employs a grid-search algorithm consisting of a sequence of successively finer nest grid searches within a spatial x, y, z volume.

On mapview shown in Figure 2(a), the microearthquake epicenters reveal a complex fault zone along a gross NE-SW striking trend which consists of narrow seismic streaks or lineations. Figure 2(b) shows the cross-sectional view projecting all the locations onto a plane perpendicular fault trend. The map indicates that all of the events are located within a depth range of 0.5 to 3.5 km. There is a relatively quiet aseismic region between 1.5 to 2.0 km. Microseismicity deep than 2.0km occurs only in the southern and northern ends of the trend. The general dip of the fault zone is steep to nearly vertical.

4. Source Mechanisms Results

The seismic source mechanisms of the microearthquakes provide important information for reservoir stress regime and geomechanical modeling. Most microearthquakes in the field are too small to generate waveforms and P-wave polarities that can be read reliably. Therefore, we only select larger events with local magnitudes greater than one. The waveforms of the 10 selected events have substantial signal-to-noise ratio. P-wave first motions are also read from the five borehole stations.

We employ the wavelet-based approach to linear waveform inversion (Sze & Toksoz, 2002) to estimate the point source mechanism. The seismic moment tensor rate functions, the linear data kernel, and the waveform data are represented by wavelet expansions, leading to a multiscale sparse matrix representation. The regularized least-squares solution is solved by the conjugated gradient method. The theoretical seismograms, or the Green's functions, are computed by the discrete wavenumber method. Vertical and radial components of the P-waveforms and polarities recorded by the five borehole stations are inverted for source mechanism.

Summaries of all inversion results are given in Figure 3. The focal mechanisms displayed in Figure 3 show that the dominant style of faulting is left-lateral strike-slip in the shallow depths less than 1.5 km. Dip-slip along obliquely trending fault predominates for deeper events (greater than 2.0km). All waveform inversion results are in good agreement with the P-wave polarities. The nearly vertical planes generally have a strike of NE-SW, indicating fault planes with a strike that is consistent with the trend of the seismicity and the surface trace.

5. Correlation of microseismicity pattern with production & injection patterns

In order to understand the relationship between the observed seismicity and hydrocarbon exploitation, we look for correlation between the seismicity pattern and production/injection operations in the field. The Natih formation is a depleting gas reservoir and pressure has dropped from 10,120 kPa to 7,920 kPa since 1973. There is oil production from the Shuaiba reservoir but pressure has been more or less maintained by water injection.

Figure 4(a) and (b) compare the overall monthly volumes of gas production and net fluid injection for the whole petroleum field. It is easy to observe that the gas production has a strong positive correlation with the microseismicity rate but not for the net fluid injection case.

In Figure 5, we plot the number of seismic events that occurred in the areas outlined by the yellow boxes and compare that number with the corresponding cumulative volumes of gas production and net fluid injection, for

the 20-month period between October 29, 1999 and June 18, 2001. In the first case (Fig 5a, c, and d), only gas production and not fluid injection (maximum correlation coefficients of 0.98 and -0.86, respectively) has high positive correlation with the microseismicity. In the second case (Fig. 5b, e, and f), both gas production and fluid injection (maximum correlation coefficients of 0.99 and 0.99, respectively) correlate highly with the microseismicity. These two areas account for 70% of the total detected events in the field and are the only areas with significant gas production whereas fluid is injected in many other parts of the area within the field. Strong correlation between injection and event rate is not observed anywhere in the field except in the second case.

6. Discussion and Conclusions

In this paper, we estimated 405 microearthquake locations in the petroleum field in Oman and these locations reveal a complex, near-vertical fault zone along a gross NE-SW striking trend. All events are located within a depth range of 0.5 to 3.5 km. The seismic moment tensors inverted by waveform inversion also show focal planes with consistent strikes and dips. The dominant styles of faulting in the field are left-lateral strike-slip in shallow depths less than 1.5 km and dip-slip along obliquely trending fault for events deeper than 2.0 km. Finally, the microseismic event rate is strongly correlated in time with the gas production.

7. Acknowledgements

References

Lomax, A., Zollo, A., Capuano, P., and Virieux, J., 2001. Precise, absolute earthquake location under Somma-Vesuvius volcano using a new 3D velocity model, Geophys. J. Int., 146, 313-331.

Sze, E.K.M. and Toksoz, M.N., 2002. Wavelet-domain regularized least-squares inversion for earthquake source parameters, 74th Annual Meeting of the Eastern Section of the Seismological Society of America, Seism. Res. Lett., 74, 68.
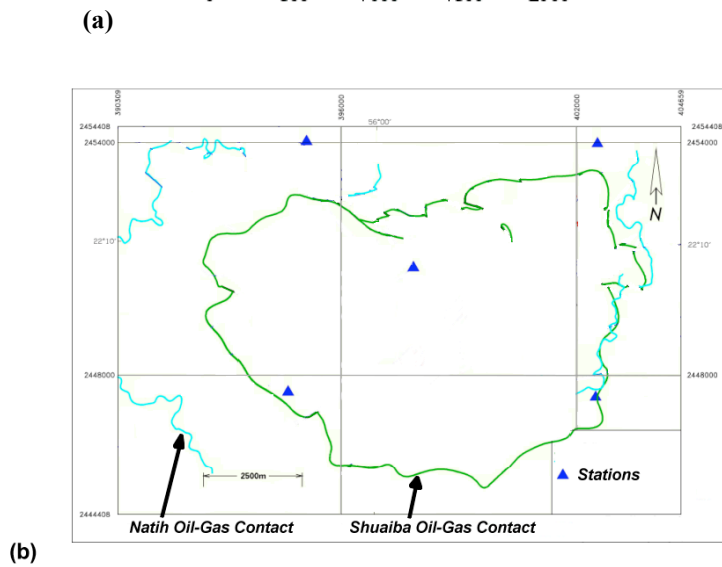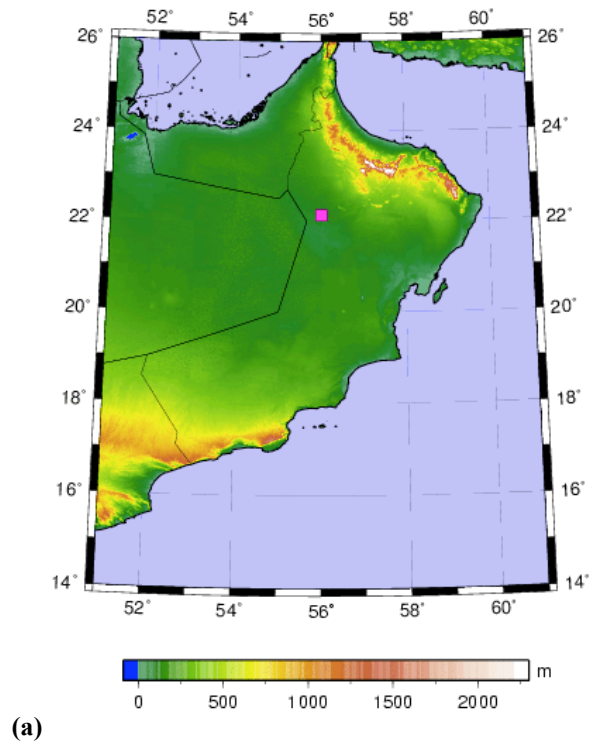
Figure 1 (a) The location of the Fahud Salt Basin and the petroleum field in Oman. (b) Map of station distribution of the downhole seismic network. Triangles denote station locations.
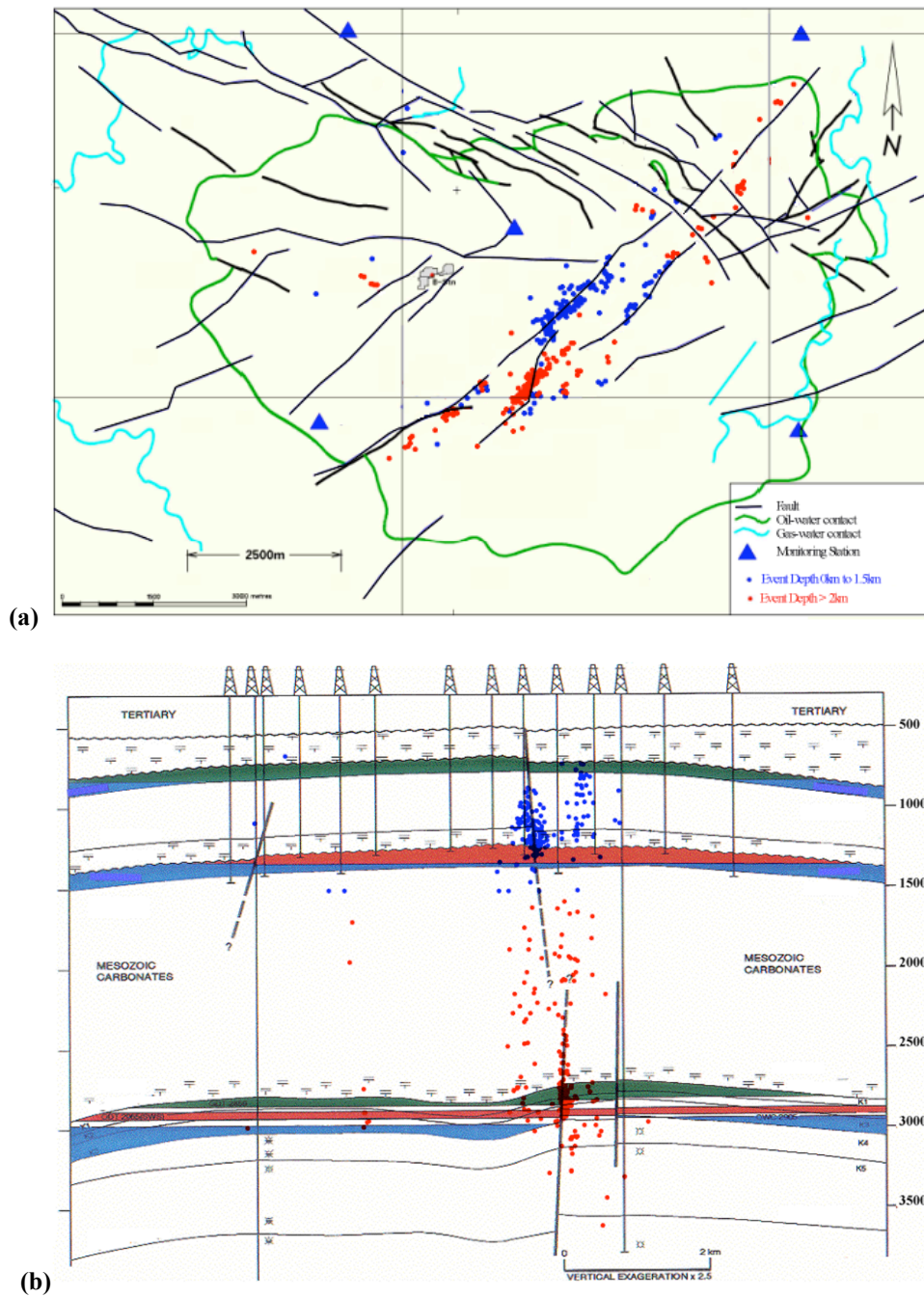
Figure 2 (a) Mapview of the 405 microearthquake locations. (b) Microearthquake locations projected onto cross-section perpendicular to the gross NE-SW trend. The shallow (<1.5 km) events are plotted in blue and the deep (>1.5km) events are plotted in red.
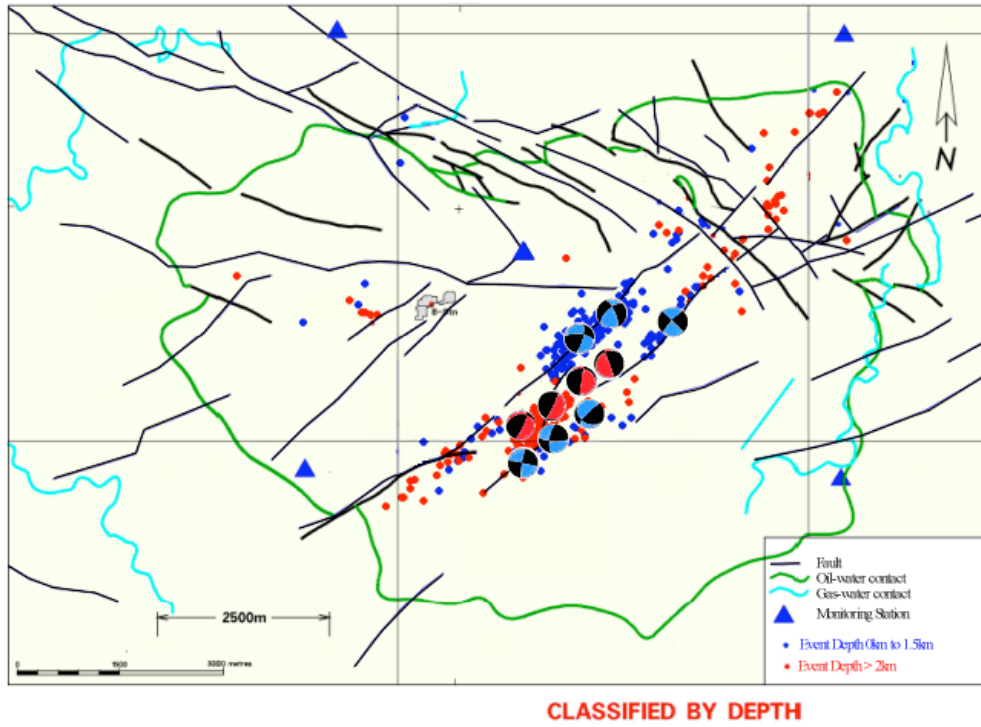
CLASSIFIED BY DEPTH

Figure 3 – Focal mechanisms of 10 microearthquakes in the petroleum field with local magnitude greater than one.
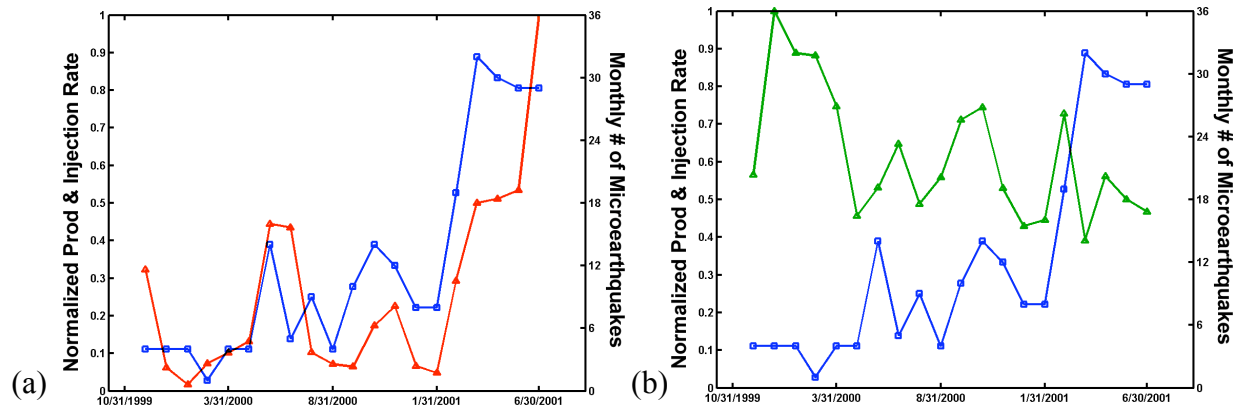

Figure 4 (a) Comparision of microseismicity pattern with gas production rates of the whole field. (b) Comparision of microseismicity pattern with net fluid injection rates of the whole field.
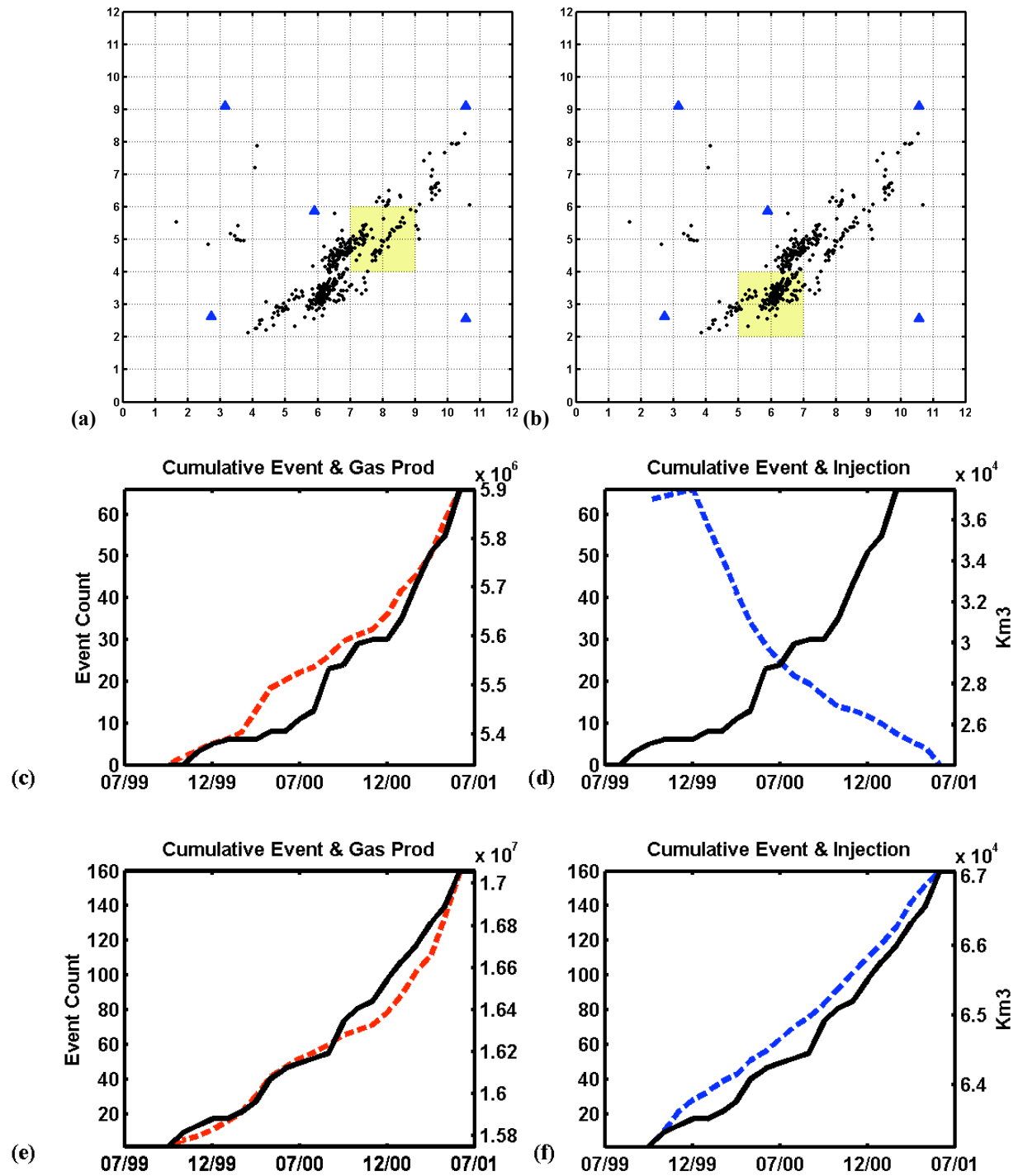
Figure 5 – The Field is divided into 2km × 2km grids. (a), (b) The yellow shaded areas indicate the selected areas for temporal analysis of seismicity and production/injection. (c) Cumulative gas production volume (red dash line) and the cumulative event counts (black line) in the study area (a). (d) Cumulative net water injection (blue dash line) and the cumulative event counts (black line) in study area (a). (e) Cumulative gas production volume (red dash line) and the cumulative event counts (black line) in the study area (b). (e) Cumulative net water injection (blue dash line) and the cumulative event counts (black line) in study area (b).